Supporting Information for

Unveiling Synergistic Effects of Interstitial Boron in Palladium-Based Nanocatalysts for Ethanol Oxidation Electrocatalysis

Lizhi Sun,[1] Hao Lv,[2] Yaru Wang,[1] Dongdong Xu,[1] and Ben Liu*,[1,2]

[1]Jiangsu Key Laboratory of New Power Batteries, Jiangsu Collaborative Innovation Center of Biomedical Functional Materials, School of Chemistry and Materials Science, Nanjing Normal University, Nanjing 210023, China. *E-mail: ben.liu@njnu.edu.cn

[2]College of Chemistry, Sichuan University, Chengdu 610064, China

Table of Contents

Figure Contents

Table Contents

1. Chemicals and Materials

Palladium (II) chloride ($PdCl_2$), copper nitrate ($Cu(NO_3)_2$), ammonium fluoride (NH_4F), boric acid (H_3BO_3), and borane dimethylamine complex (DMAB) were obtained from Alfa Aesar. Commercial Pd/C (30 wt. %) and Nafion solution (5 wt. % in alcohol and H_2O) were purchased from Sigma Aldrich. Nitrogen-functionalized graphene (N-G with N content of 3.0-5.0 wt %) were purchased from Nanjing XFNANO Materials Tech Co. Ltd. Ethanol, hydrazine hydrate (N_2H_4, 50%), and potassium hydroxide (KOH) were obtained from Sinopharm Chemical Reagent Co. Ltd. (Shanghai). To prepare 10 mM (mmol L^{-1}) H_2PdCl_4 solution, 0.355 g of $PdCl_2$ was dissolved with 20 mL of 0.2 M HCl solution in a 200 mL volumetric flask and further diluted to 200 mL by deionized H_2O. All the reagents are of analytical reagent grade and used without further purification. Deionized H_2O with the resistivity of 18.25 mΩ was used in all experiments.

2. Synthesis of ternary PdB@N-G and PdCuB@N-G as well as their counterparts

Binary PdB and ternary PdCuB nanoparticles on N-G (PdB@N-G and PdCuB@N-G) were synthesized by a solution-phase route, in which H_2PdCl_4 (and $Cu(NO_3)_2$), DMAB and H_3BO_3, and N-G were served as metal precursors, the B sources, the functional support, respectively. DMAB and H_3BO_3 were also behaved as the co-reducing agents to drive the crystalline growth of ternary PdCuB alloys. The synthetic temperatures were fixed at 95 ^{o}C. In a typical synthesis of PdCuB@N-G, 1.0 mL of 0.0338 M NH_4F, 1.0 mL of 0.101 M H_3BO_3, 0.5 mL of 10 mM H_2PdCl_4, and 0.5 mL of 10 mM $Cu(NO_3)_2$ were carefully added into 10 mL of deionized H_2O. Then, 0.4 mL of 1.0 mg mL^{-1} N-G was injected into the above solution and further incubated at 95 ^{o}C for 30 min. Subsequently, 1.0 mL of freshly prepared 0.1 M DMAB was quickly injected with gentle shaking. The color of the solution was immediately turned to black, implying the formation of PdCuB alloys. After kept the reaction vial at 95 ^{o}C for another 2 h, the product was collected by centrifuged and washed several times with ethanol/H_2O. In contrast, **PdB@N-G** was synthesized by using H_2PdCl_4 as the sole metal precursor. As the controls, **metallic Pd NPs@N-G** and **bimetallic PdCu NPs@N-G** were obtained with the same procedures but using N_2H_4 as the reducing agent.

3. The preparation of nanocatalysts ink

Before electrochemical tests, the nanocatalysts and work electrode [glassy carbon electrode (GCE, 0.07065 cm^2)] were totally cleaned with H_2O/ethanol. The ink of the catalyst was prepared as followed: 1.0 mg of nanocatalyst was mixed into 0.75 mL of ethanol and 0.25 mL of H_2O, and further sonicated for 30 min. Then, 50 µL of Nafion solution (5 wt. % in alcohol and H_2O) was injected and further sonicated for another 30 min. Last, 3.0 µL of the prepared ink solution (~ 3 µg of catalyst) was directly casted on the GCE electrode and dried at 40 °C before the tests.

4. Electrochemical ethanol oxidation reaction

All the electrocatalytic tests were repeated more than five times. Electrocatalytic studies were carried out on a CHI 660E electrochemical analyzer with a three-electrode system in which a GCE was used as working electrode, a carbon rod as counter electrode, and a silver/silver chloride electrode as reference electrode. The potentials used in this work were reported with respect to the saturated calomel electrode (SCE). The cyclic voltammogram (CV) was continuously scanned until a stable curve was obtained for further removal of the surfactant in N_2-saturated 1.0 M KOH. The mass activity of the nanocatalyst for the electrooxidation of ethanol was collected by scanning CV in 1.0 M KOH and 1.0 M ethanol at a scan rate of 50 mV s^{-1}. For electrochemical CO stripping tests, the catalysts electrode was first immersed in 1.0 M KOH, followed by purging with CO at 0.15 V for 30 min (full coverage of CO on the catalysts). Then, the electrode was moved to 1.0 M KOH for electrochemical CO stripping measurements in the potential range between -0.6 V and 0 V.

Electrochemical active surface areas (ECSAs) of the nanocatalysts were calculated from CVs in the area of PdO reduction peaks with a scan rate of 50 mV s^{-1}: $\mathrm{ECSA} = \frac{\mathrm{Q}_{\mathrm{PdO}}}{0.405\ \mathrm{mC\ cm}^{-2} \times \mathrm{m}_{\mathrm{Pd}}}$, where Q_{PdO} is the charge by integrated the reduction peak area of PdO to Pd, 0.405 mC cm^{-2} is the charge for the reduction of PdO, and m_{Pd} is the mass of Pd on the electrode. The activation energy (E_a) values of the nanocatalysts were calculated based on Arrhenius equation as follows: $\mathrm{I} = \mathrm{A}e^{-\frac{E_a}{\mathrm{RT}}}$, where I is the current at a specific potential, R is the gas content (8.315 J mol^{-1} K^{-1}), T is the test temperature in K, and E_a is the apparent activation energy at a specific potential.

5. Characterizations

Transmission electron microscopy (TEM) observations were performed at 200 kV using a JEOL JEM-2100 microscope. TEM samples were prepared by casting a sample suspension onto a carbon coated nickel grid (300 mesh). Wide-angle X-ray diffraction (XRD) patterns were obtained on powder samples using a D/max 2500 VL/PC diffractometer (Japan) equipped with graphite-monochromatized Cu Kα radiation. X-ray photoelectron spectroscopy (XPS) was performed using a scanning x-ray probe of Al Kα radiation (thermal ESCALAB 250 Xi). The binding energy of the C 1s peak (284.8 eV) is used as a criterion for calibrating the binding energy of other elements. Inductively coupled plasma mass spectrometry (ICP-MS) was recorded on a NexION 350D. Gas chromatography-mass spectrometry (GC-MS) was studied on an Agilent 7820A GC system connected with a thermal conductivity detector of 5974 series MSD.

6. Supporting Figures and Tables

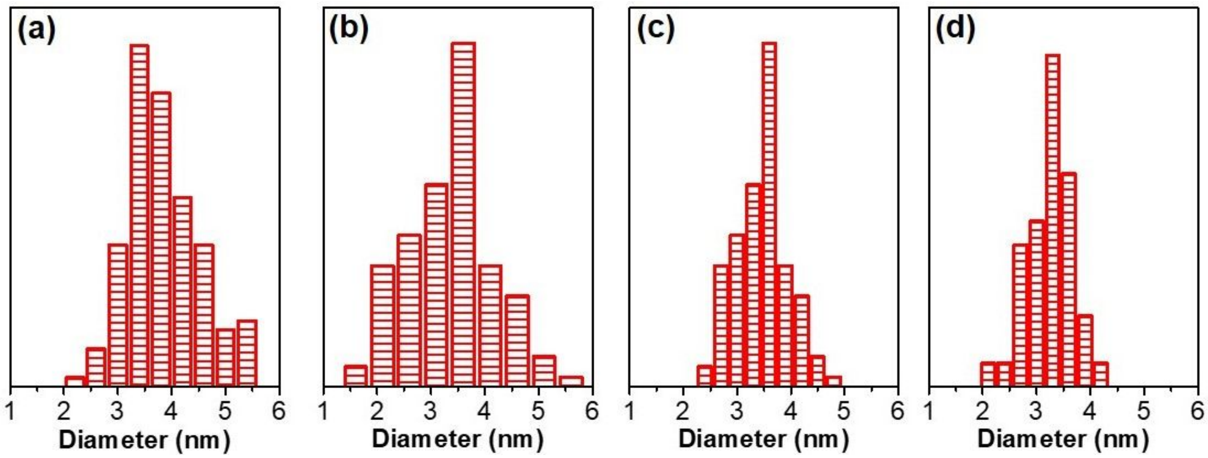

Figure S1. Size distributions of (a) Pd@N-G, (b) PdB@N-G, (c) PdCu@N-G, and PdCuB@N-G.

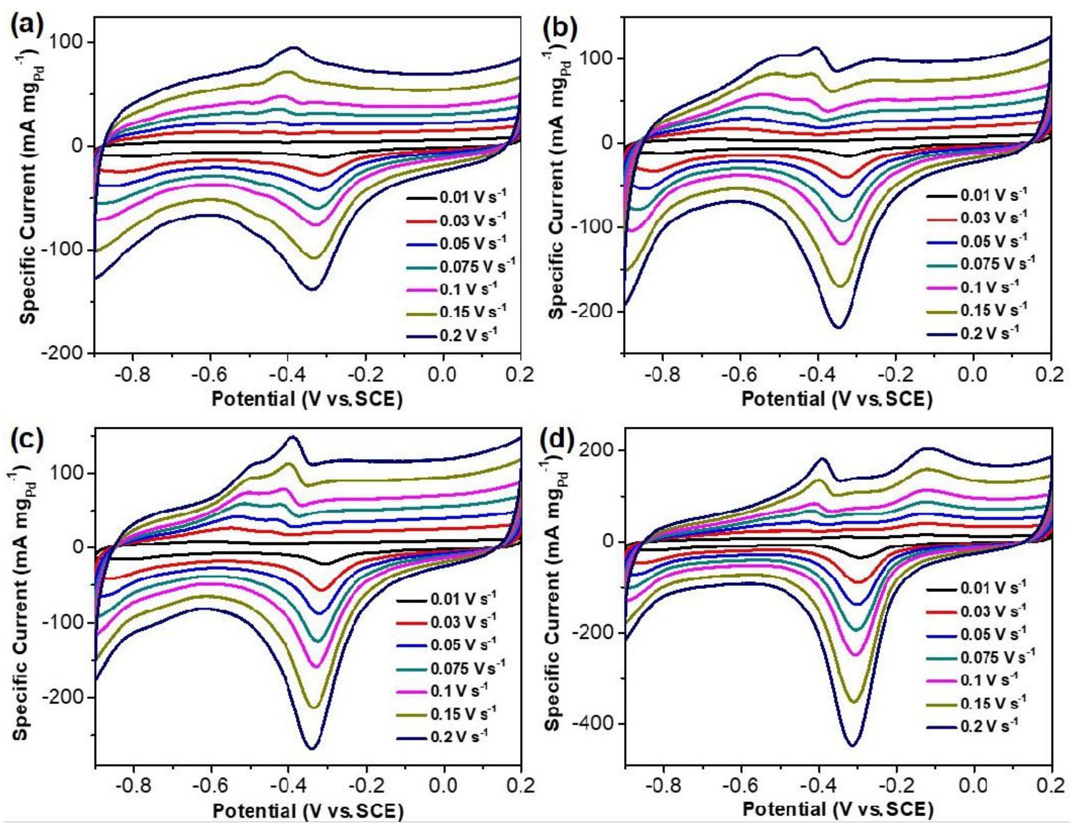

Figure S2. CV curves of (a) Pd/C, (b) Pd@N-G, (c) PdB@N-G, and (d) PdCu@N-G collected in 1.0 M KOH with different scan rates.

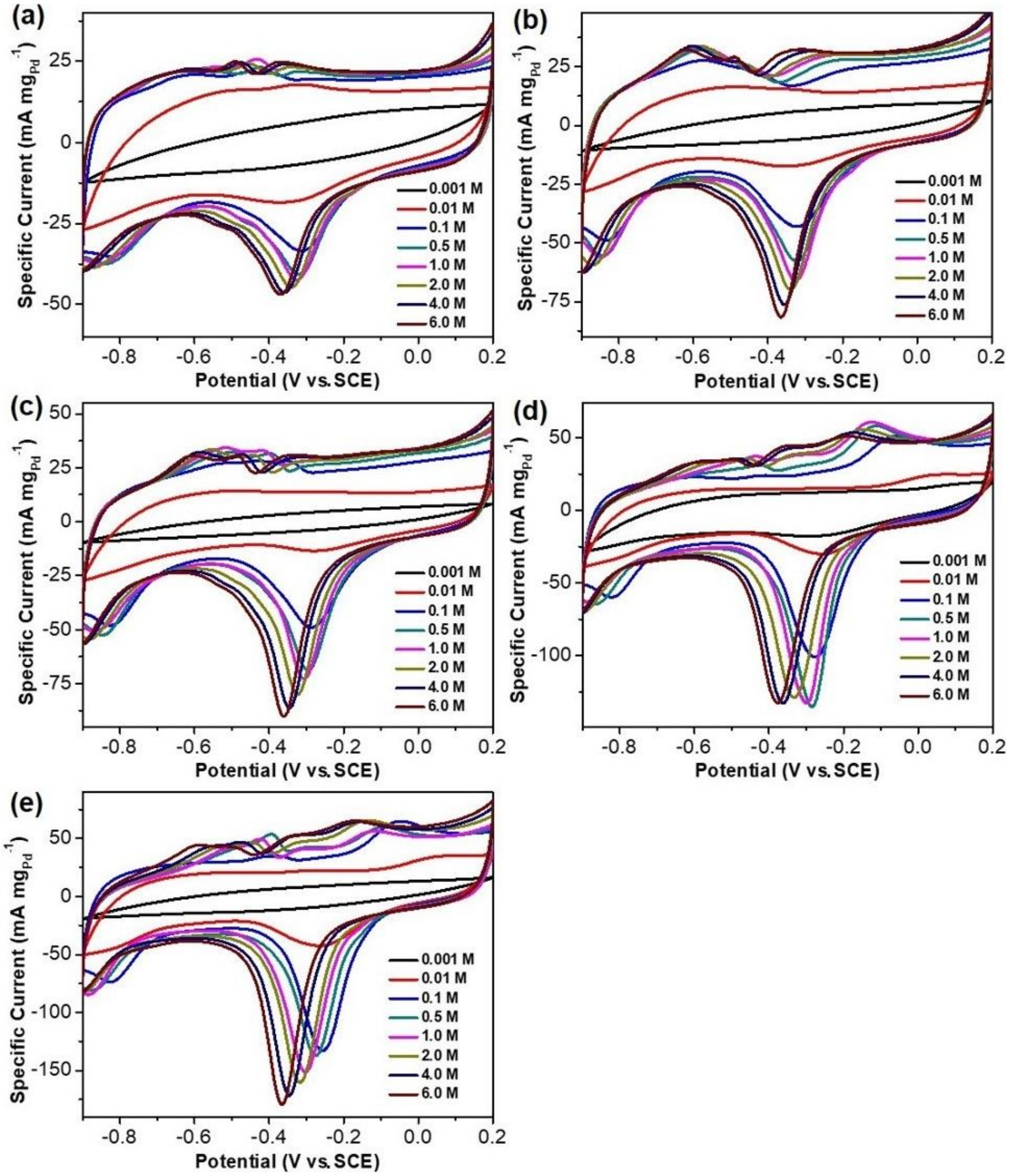

Figure S3. CV curves of (a) Pd/C, (b) Pd@N-G, (c) PdB@N-G, (d) PdCu@N-G, and (e) PdCuB@N-G collected in different KOH concentrations (50 mV s^{-1}).

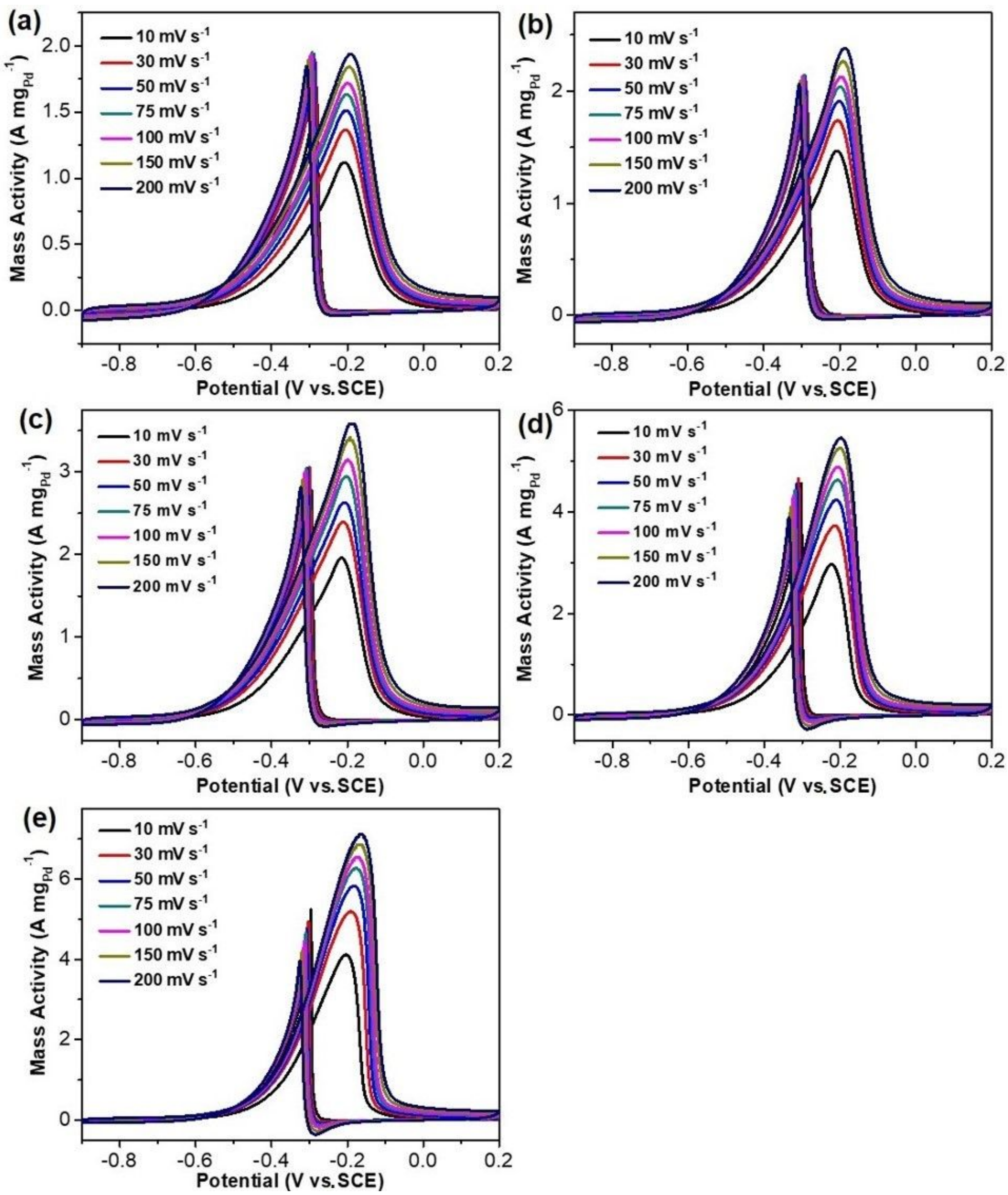

Figure S4. CV curves of (a) Pd/C, (b) Pd@N-G, (c) PdB@N-G, (d) PdCu@N-G, and (e) PdCuB@N-G collected in 1.0 M KOH and 1.0 M ethanol with different scan rates.

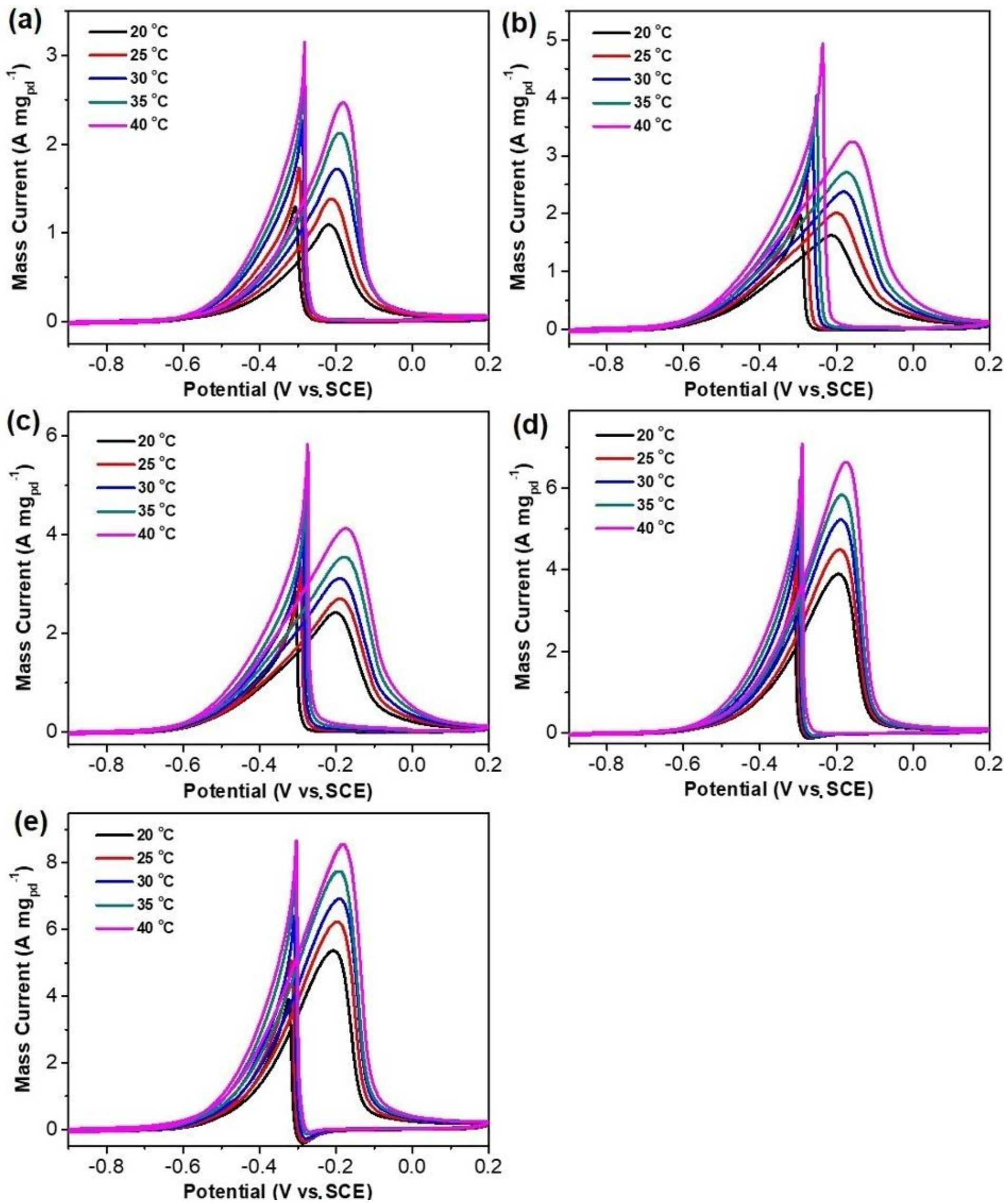

Figure S5. CV curves of (a) Pd/C, (b) Pd@N-G, (c) PdB@N-G, (d) PdCu@N-G, and (e) PdCuB@N-G collected in 1.0 M KOH and 1.0 M ethanol with different test temperatures.

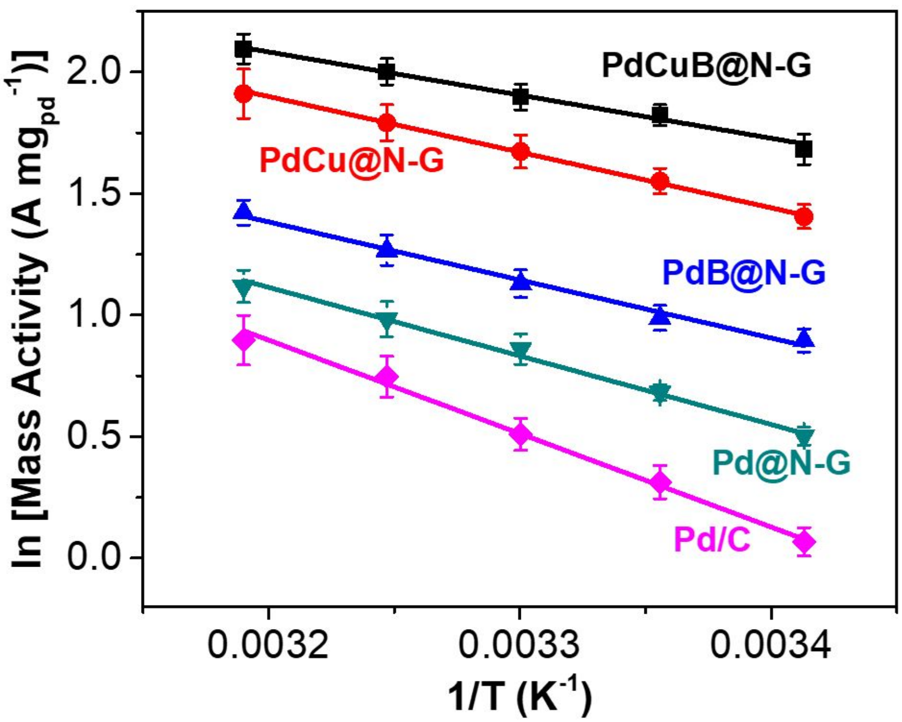

Figure S6. The relationship between mass activities and test temperatures for (a) Pd/C, (b) Pd@N-G, (c) PdB@N-G, (d) PdCu@N-G, and (e) PdCuB@N-G (The results were summarized from Figure S5).

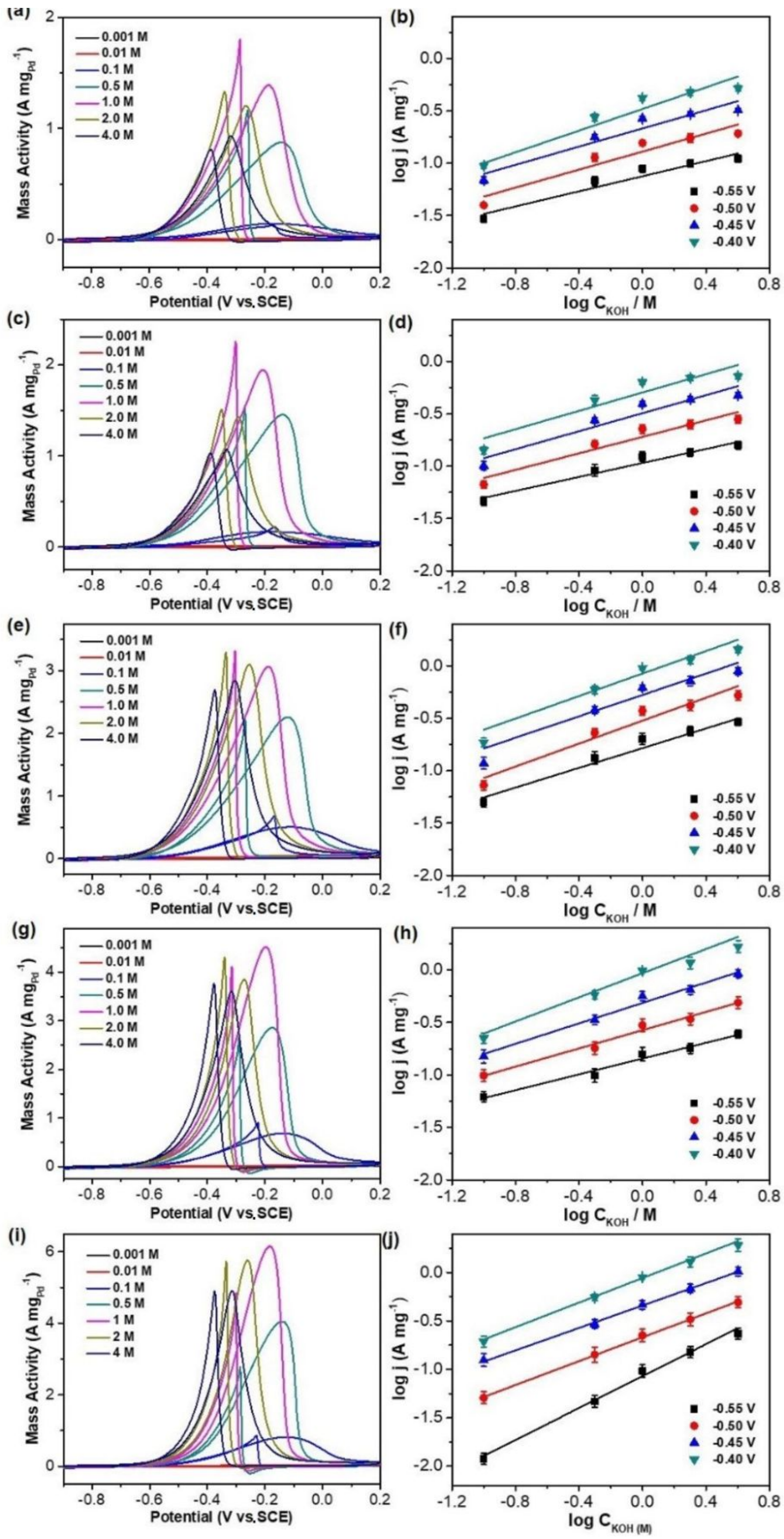

Figure S7. (a,c,e,g,i) CV curves and (b,d,f,h,j) corresponding relationships between $\log_j$ and $\log C_{KOH}$ at different potentials for (a,b) Pd/C, (c,d) Pd@N-G, (e,f) PdB@N-G, (g,h) PdCu@N-G, and (i,j) PdCuB@N-G collected in 1.0 M ethanol with different KOH concentrations.

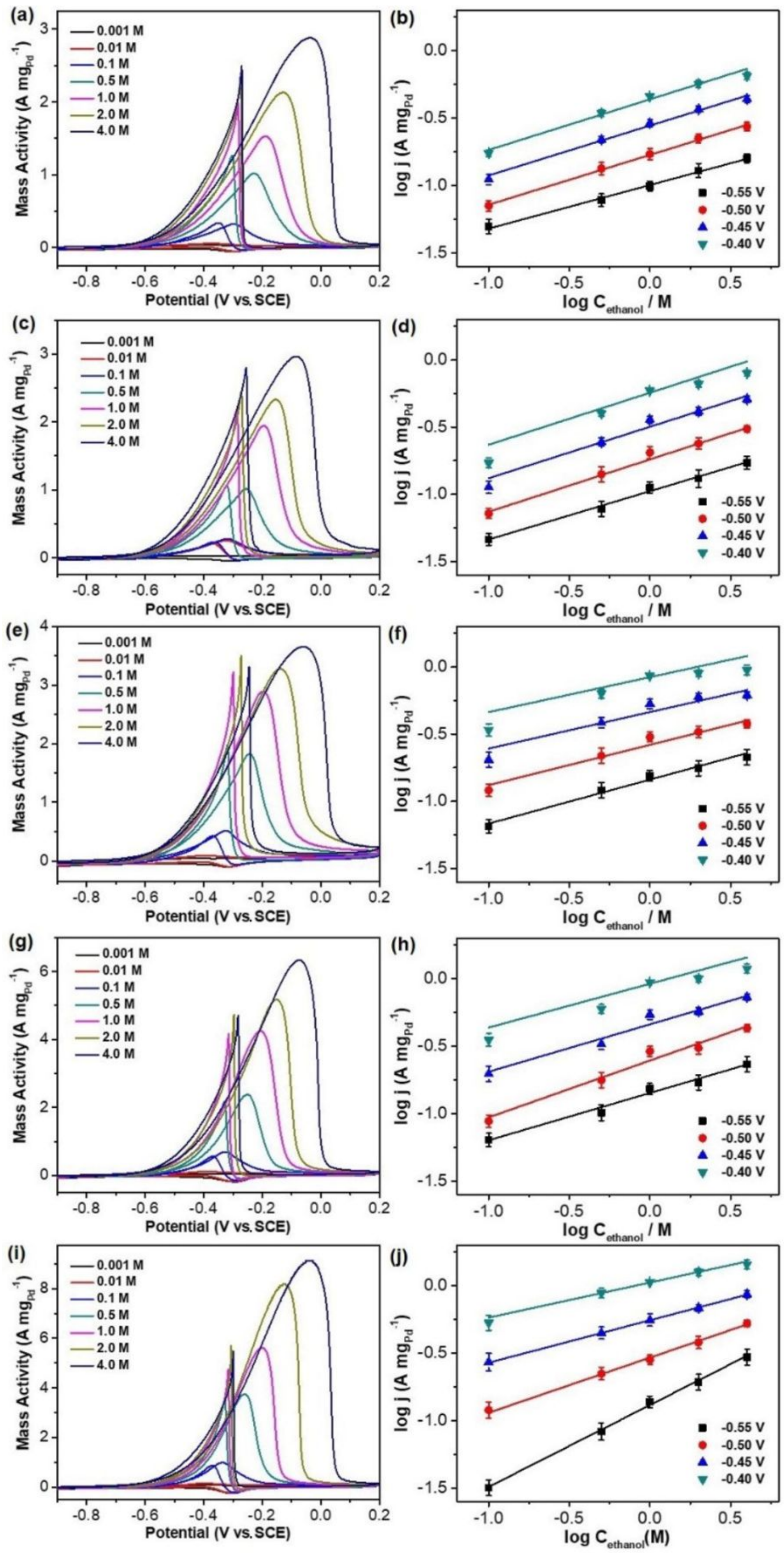

Figure S8. (a,c,e,g,i) CV curves and (b,d,f,h,j) corresponding relationships between $\log_j$ and $\log C_{ethanol}$ at different potentials for (a,b) Pd/C, (c,d) Pd@N-G, (e,f) PdB@N-G, (g,h) PdCu@N-G, and (i,j) PdCuB@N-G collected in 1.0 M KOH with different ethanol concentrations.

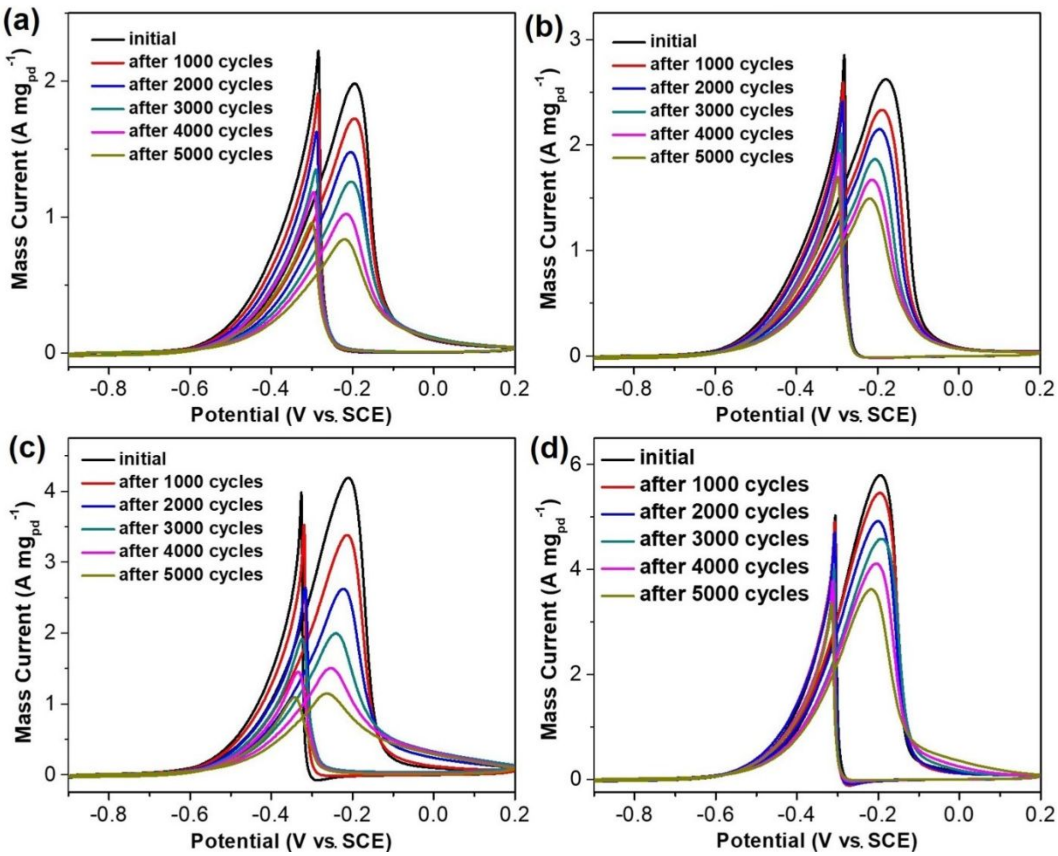

Figure S9. CV curves of (a) Pd@N-G, (b) PdB@N-G, (c) PdCu@N-G, and (d) PdCuB@N-G collected in 1.0 M KOH and 1.0 M ethanol for 5000 cycles.

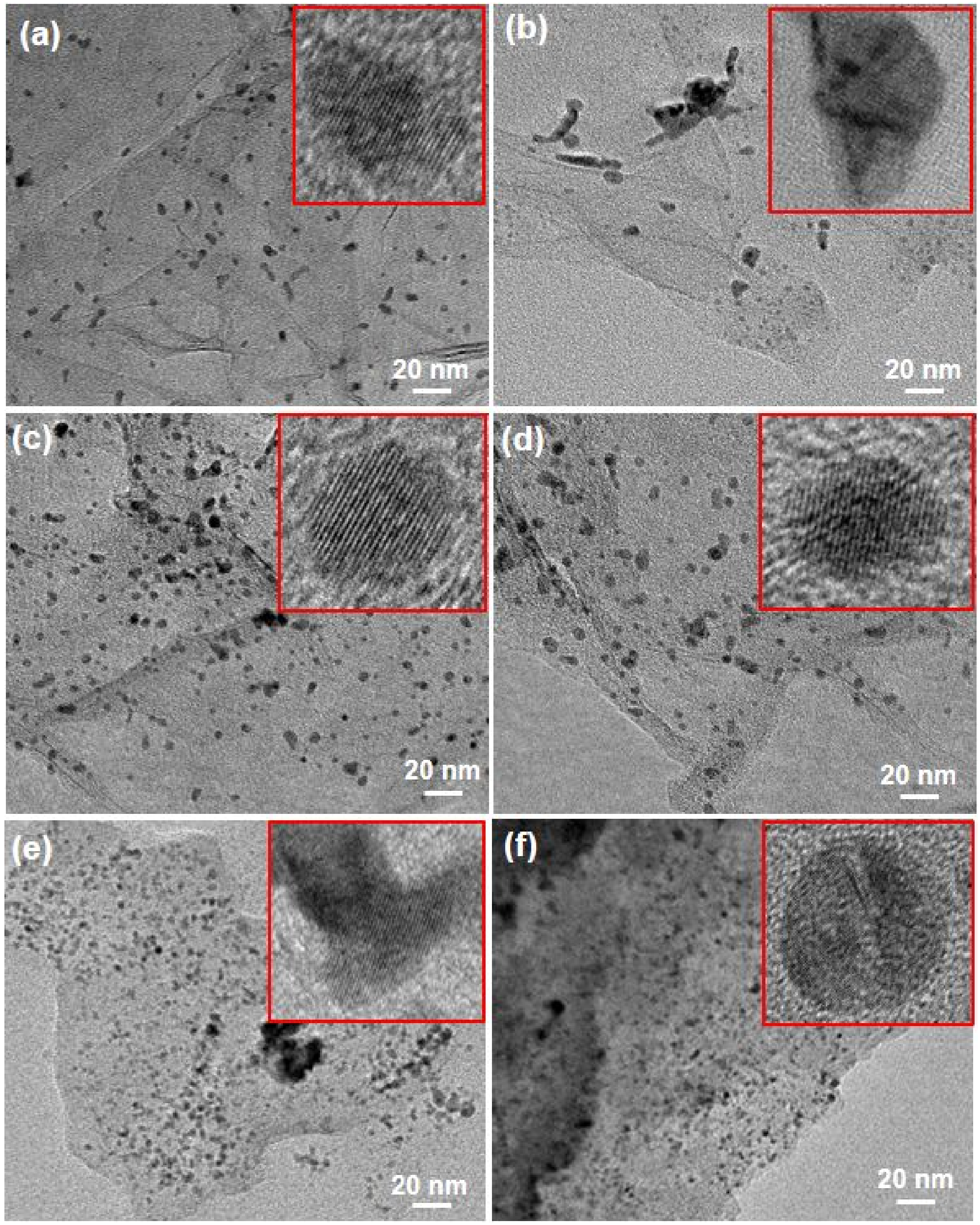

Figure S10. TEM and (insets) high-resolution TEM images of (a) PdCuB@N-G, (c) PdCu@N-G, (c) PdB@N-G, (d) Pd@N-G, and (e) Pd/C after EPR stability tests. (f) TEM and (inset) high-resolution TEM images of fresh Pd/C.

Table S1. Elemental compositions of B-alloyed Pd-based nanocatalysts before and after stability tests collected with ICP-MS.

Samples	Pd@N-G	PdB@N-G	PdCu@N-G	PdCuB@N-G
Pd/Cu/B ratios (fresh samples)	100 : 0 : 0	92.0 : 0 : 8.0	51.1 : 48.9 : 0	46.3 : 45.7 : 8.0
Pd/Cu/B ratios (after tests)	100 : 0 : 0	91.9: 0 : 8.1	55.3 : 44.7 : 0	49.3 : 42.8 : 7.9

Notes for Table S1: The B amounts in fresh PdB@N-G and PdCuB@N-G are 8 at. %. Pd/Cu ratios in PdCu@N-G and PdCuB@N-G are ~1:1, which are almost same to the feed ratios of H_2PdCl_2 and $Cu(NO_3)_2$ (1:1). After EOR stability tests, B amounts in both PdB@N-G and PdCuB@N-G are still 8 at. %, indicating the high structural stability.

Table S2. Summarizations of the activities of Pd-based nanocatalysts in EOR electrocatalysis.

Nanocatalysts	Measurement Conditions		Mass Activity ($A\ mg_{NM}^{-1}$)	References
	CH_3CH_2OH (M)	KOH (M)		
PdCuB @N-G	**1.0**	**1.0**	**5.83**	**This work**
c-Pd-Ni-P@a -Pd-Ni-P	1.0	1.0	3.05	*Adv. Mater.* **2020**, *32, 2000482*
Pd/amorphous-$SrRuO_3$	1.0	1.0	4.0	*Nano Energy* **2020**, *67, 104247*
Pd_3Pb/C	0.5	0.5	2.05	*Chem. Mater.* **2020**, *32, 2044*
CoP/RGO-Pd	1.0	1.0	4.597	*ACS AMI* **2020**, *12, 28903*
Cu-Pd/Ir@$Au_{1/6ML}$ NSs	1.0	1.0	3.583	*ACS AMI* **2020**, *12, 25961*
PdAgCu BMSs	1.0	1.0	6.36	*Nano Lett.* **2019**, *19, 3379*
PdCuP NWs	1.0	1.0	6.7	*Appl. Catal. B Environ.* **2019**, *253, 271*
$Pt_{56}Cu_{28}Ni_{16}$	1.0	1.0	5.6	*Nano Lett.* **2019**, *19, 5431*
PdBP MSs	1.0	1.0	3.65	*ACS Nano* **2019**, *13, 12052*
PdP_2/rGO	0.5	0.5	1.6	*Appl. Catal. B Environ.* **2019**, *242, 258*
PdAgCu MSs	1.0	1.0	4.64	*Chem. Sci.* **2019**, *10, 1986*
PdPtCu NSs	1.0	1.0	2.67	*Green Chem.* **2019**, *21 , 2367*
Pd-$WO_{2.75}$ NB	1.0	1.0	1.98	*ACS AMI* **2019**, *11, 10028*
Pt_5FePd_2 NWs	1.0	1.0	4.965	*ACS AMI* **2019**, *11, 30880*
$Pt_{54}Rh_4Cu_{42}$ CNBs	1.0	1.0	4.09	*Adv. Energy Mater.* **2018**, *8, 1801326*
PdAgCu HMSs	1.0	1.0	5.13	*ACS Cent. Sci.* **2018**, *4, 1412*
Pd/NiSA	1.0	1.0	1.20	*Chem. Commun.* **2018**, *54, 12404*
PdNi HNCs	1.0	1.0	1.201	*Nano Energy* ***2017***, *42, 353*
$PtPd_3Ag_5$/C-D	1.0	1.0	4.5	*Electrochim. Acta* **2017**, *236, 72*
Pd/$Ni(OH)_2$/rGO	1.0	1.0	1.546	*Adv. Mater.* **2017**, *29, 1703057*
v-PdCuCo-AS	1.0	1.0	0.823	*Adv. Mater.* **2017**, *30, 1704171*
Pd NN	1.0	1.0	2.04	*ACS AMI* **2017**, *9, 39303*
3D PdCu NSs	1.0	1.0	4.3	*Small* **2017**, *13, 1602970*
$Pd_{68}Cu_{32}$ Aerogels	1.0	1.0	3.472	*Adv. Mater.* **2016**, *28, 8779*
$PdCu_2$ NPs	.1.0	1.0	1.63	*ACS AMI* **2016**, *8, 34497*
Au NR_{core}-Pt/Pd_{shell}	1.0	1.0	2.5	*J. Mater. Chem. A* **2016**, *4, 3765*